equations. A closed-form solution can be obtained if Eq. (4) is treated as a singular perturbation problem where the limiting form of the equation is obtained through the use of the following transformations:

$$\bar{G} = (|\beta|)^{1/2}G \quad \text{and} \quad \bar{\eta} = (|\beta|)^{1/2}\eta$$

Dividing the resulting equation by β and taking the limit for large β gives

$$\bar{G}''' - A\sigma(\bar{G}'^2 + 2B\bar{G}') = 0$$

where $\sigma = \beta/|\beta|$. This equation can be integrated twice in closed form using the boundary conditions that as $\bar{\eta} \to \infty$, $\bar{G}' \to 0$, $\bar{G}'' \to 0$, and $\bar{\eta} = 0$, $\bar{G}' = 1$ to give (note that $AB\sigma = |B|$):

$$\bar{G}' = 3B[\tanh^2\{(|B|/2)^{1/2}\eta + \tanh^{-1}[(\tfrac{1}{3}B+1)]^{1/2}\} - 1] \quad (5)$$

where $B \leqq -\frac{1}{3}$ and $\bar{G}' > 0$. Equation (5) is a generalization of the converging channel flow problem[8] ($B = -1$) to include the moving wall situation. The $B = -\frac{1}{3}$ limit agrees with the results of Steiger and Chen and has the following velocity distribution

$$\bar{G}' = 1 - \tanh^2[\bar{\eta}/(6)^{1/2}]$$

Algebraic Decay Solutions

The limiting cases at $B = -\frac{1}{3}$, $\beta = -\infty$, and $B = 0$, $\beta = -1$ are connected by a set of solutions involving asymptotic algebraic decay of G' with $\bar{\eta}$. The asymptotic form of G' at large η with $AB < 0$ and $\beta < 0$ can be written as (following techniques discussed in Ref. 9):

$$G'(\eta) \sim [(|AB|)^{1/2}(\eta - \delta^*/B)]^{2\beta}$$

These solutions have infinite displacement thicknesses for $\beta \geqq -\frac{1}{2}$ but are well behaved for smaller β. For $-1 > \beta > -\frac{1}{2}$ the solutions are difficult to numerically compute because of the large algebraic tail. Solutions were obtained at $\beta = -1.1$, -1.5, and -2.0 over a range of B and were used to determine the value of B for $G''(0) = 0$ by interpolation; the results are shown in Fig. 1.

Limit $u_w = u_e$

The fact that the wakelike solutions ($B < -1$) or the jetlike solutions ($B > 0$) have a limiting point at $B = \pm\infty$ and $\beta = -\frac{1}{2}$ has been recognized by other investigators. At that point $u_w = u_e$ and thus $u \equiv u_e$ throughout the boundary layer so long as G' is finite. Although the velocity distributions are degenerate, the limiting case may have some interest. If the limiting case is considered as a singular perturbation problem where the singularity is removed by the transformations

$$G(\eta) = F(\eta_1)/(|AB|)^{1/2} \quad \text{and} \quad \eta = \eta_1/(|AB|)^{1/2}$$

one finds that the equation for $F(\eta_1)$ is identical to the large η_1 approximation, i.e.,

$$F''' + \eta_1 F'' - 2\beta F' = 0, \quad F'(\eta_1) \equiv dF/d\eta_1 \quad (6)$$

A series solution of the following form can be assumed:

$$F' = K\eta_1^{\gamma}\exp(m\eta_1^2)\sum_{n=1}^{\infty} p_n/\eta_1^n$$

The result, which has been derived in Ref. 7, has special properties at certain values of β given by

$$\beta_n = -(2n-1)/2, \qquad n = 1, 2, 3, \ldots$$

The series then reduces to a finite number of terms and can be made to satisfy the inner as well as outer boundary conditions. Some of these solutions are given in Table 1.

Table 1 Limiting solutions for $F''(0) = 0$

n	β_n	$F'(\eta_1)$
1	$-\frac{1}{2}$	$\exp(-\eta_1^2/2)$
2	$-\frac{3}{2}$	$(1-\eta_1^2)\exp(-\eta_1^2/2)$
3	$-\frac{5}{2}$	$(1-2\eta_1^2+\eta_1^4/3)\exp(-\eta_1^2/2)$
...	...	...
...	...	...

The $n = 2$ case corresponds to the limiting case for a Libby-Liu[10] family of solutions with boundary-layer velocity overshoot. The $G''(0) = 0$ solutions for this family are indicated as a dashed line in Fig. 1 because the $B = -1$ point is the only other value currently available. Higher n's correspond to the larger negative β families whose existence was noted by Libby-Liu.[10] Solutions to Eq. (6) may be obtained for any β by numerical integration; however, $G''(0)$ is infinite for all β (except at β_n) because $G''(0) = (|AB|)^{1/2}F''(0)$. These results for the limiting case may be used to determine the large B approximations in a perturbation series approach similar to that used by Mirels[11] for $\beta = 0$; one has

$$G(\eta, B) = [1/(|B|)^{1/2}]F[(|B|)^{1/2}\eta] + 0(1/|B|)$$

References

[1] Stewartson, K., "Further Solutions of the Falkner-Skan Equation," *Proceedings of the Cambridge Philosophical Society*, Vol. 50, 1954, pp. 454–465.

[2] Kennedy, E. D., "Wake-Like Solutions of the Laminar Boundary-Layer Equations," *AIAA Journal*, Vol. 2, No. 2, Feb. 1964, pp. 225–231.

[3] Steiger, M. H. and Chen, K., "Further Similarity Solutions of Two-Dimensional Wakes and Jets," *AIAA Journal*, Vol. 3, No. 3, March 1965, pp. 520–528.

[4] Schlichting, H., "Laminare Strahlausbreitung," *Zeitschrift für angewandte Mathematik und Mechanik*, Vol. 13, 1933, pp. 260–263.

[5] Goldstein, S., "On Backward Boundary Layers and Flow in Converging Passages," *Journal of Fluid Mechanics*, Vol. 21, Pt. 1, 1965, pp. 33–45.

[6] Brown, S. N. and Stewartson, K., "Similarity Solution of Boundary-Layer Equations with Algebraic Decay," *Journal of Fluid Mechanics*, Vol. 23, 1965, pp. 673–687.

[7] Danberg, J. E. and Fansler, K. S., "Similarity Solutions of the Boundary Layer Equations for Flow Over a Moving Wall," BRL Rept., 1973, U.S. Army Ballistic Research Labs., Aberdeen Proving Ground, Md.

[8] Pohlhausen, D., "Zur naherungsweisen Integration der Differentialgleichung der Grenzschicht," *Zeitschrift für angewandte Mathematik und Mechanik*, Vol. 1, 1921, p. 252.

[9] Rosenhead, L., ed., *Laminar Boundary Layers*, Oxford Univ. Press, Oxford, England, 1963, p. 247.

[10] Libby, P. A. and Liu, T. M., "Further Solutions of the Falkner-Skan Equations," *AIAA Journal*, Vol. 5, No. 5, May 1967, pp. 1040–1042.

[11] Mirels, H., "Laminar Boundary Layer Behind Shock Advancing into Stationary Fluid," TN 3401, March 1955, NACA.

Inverse Relationships in Equilibrium Statistical Thermodynamics

LAWRENCE BAYLOR ROBINSON* AND TIEN TSAI YANG†
University of California, Los Angeles, Calif.

I. Introduction

EMPIRICAL (sometimes called classical or phenomenological) thermodynamics provides relationships among physical quantities. Statistical thermodynamics provides methods of calculating the physical quantities within the framework of specified atomic models. Such relationships may be called *direct relationships*. It is usually rather difficult to go in the opposite direction, namely to determine a specific model from a series of measured values of some physical quantity. The

Received March 13, 1974; revision received April 22, 1974.
Index category: Thermophysics and Thermochemistry.

* Professor of Engineering and Applied Science.
† Research Engineer, School of Engineering and Applied Science. Member AIAA.

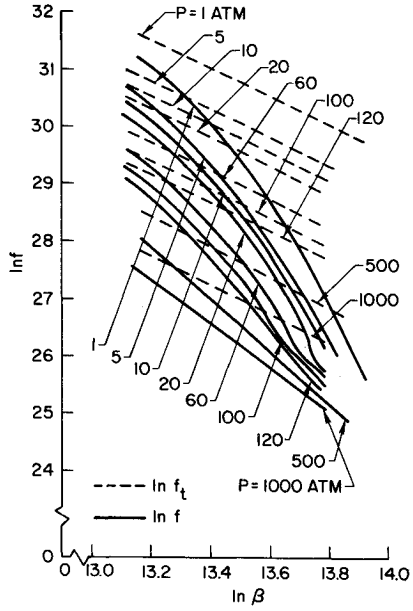

Fig. 1 Partition function of argon gas as a function of temperature and pressure.

measured quantity is usually consistent with more than one atomic model. Relationships which give the atomic model in terms of the measured thermodynamic quantities may be called *inverse relationships*. Many times, the forward direction is a smoothing process, whereas the reverse is not. Under such circumstances information is lost in inverse relationships. The purpose of this present Note is to examine some inverse relationships in which the reliability and accuracy are the same as in the direct relationships of statistical thermodynamics.

In statistical thermodynamics, the concept of partition function plays a central conceptual role. In principle it can be calculated from quantum mechanical considerations. Once the partition function is calculated, all other thermodynamic properties can be obtained from it. If, however, the partition function is measured, it is possible to make some remarks about the kind of quantum mechanical system which is involved. One cannot determine the microscopic system uniquely; nevertheless some possibilities can be ruled out.

Surprising as it seems, no listing of an experimentally determined partition function could be found. Most experimentalists are interested in other thermodynamic properties such as free energy and also pressure-volume data. These latter measurements are required in a determination of the partition function. Since the practical value of having a partition function is to obtain an easy excess to the other properties, tabulations of the partition function are not made.

We are interested in having an experimentally determined partition function for three reasons: 1) to find an analytical form and compare it with theory, 2) to find out something about the microscopic system, and 3) to find an analytical expression for the equation of state of the system in question.

We have chosen argon gas as the system to be investigated. It has the advantage of being a monatomic gas without the complicated quantum effects associated with helium. The data used in our calculations were reported by F. Din[1] and covered the temperature range from 110°K to 500°K and pressures from 1–2000 atm.

The partition function for one particle can be written in one of two ways as shown immediately below, viz.,[2]

$$f = \Sigma_i g_i e^{-\beta E_i} \tag{1}$$

or

$$f = (1/h^3)\int\int\cdots\int e^{-\beta E}\, d\mathbf{p}\, d\mathbf{r} \tag{2}$$

where E is the total energy of the particle.

It has been demonstrated over and over that it is useful to write the partition function Z for a system of N particles as

$$Z = Z_{tr} Z_c \tag{3}$$

where Z_{tr} is the translational part and Z_c is the configurational part. Since Z_{tr} is known, our method provides an indirect way of calculating Z_c, which will be written out more explicitly shortly.

II. Configuration Integral

First we note that for N nonlocalized particles

$$Z = \frac{1}{N!}\int\int\cdots\int \exp[-\beta H(\mathbf{p},\mathbf{q})]\, d\mathbf{p}_1\, d\mathbf{p}_2 \ldots d\mathbf{q}_{N-1}\, d\mathbf{q}_N \tag{4}$$

which can be simplified to

$$Z = \left(\frac{1}{N!}\frac{2\pi m}{\beta h^2}\right)^{3N/2} Z_c \tag{5}$$

where

$$Z_c = \int\int\cdots\int e^{-\beta U}\, d\mathbf{r}_1\, d\mathbf{r}_2 \ldots d\mathbf{r}_N \tag{6}$$

This configurational partition function can be calculated in principle. For our purposes, it is convenient to define a new function $f_c(\beta, p)$ in terms of the numerical value of Z_c. We write[3]

$$Z_c = [f_c(\beta, p)V]^N \tag{7}$$

For a system of N nonlocalized and independent particles, the total partition function Z can be written in terms of f as follows:

$$Z = \frac{1}{N!}\left(\frac{2\pi m}{\beta h^2}\right)^{3N/2} [f_c(\beta, p)]^N \tag{8}$$

The thermodynamic function, Helmholtz free energy A, can be expressed in terms of Z in a simple fashion, namely

$$A \equiv -kT\ln Z \equiv -kT\ln(f^N/N!) = -NkT\ln f + kT\ln N! \tag{9}$$

If we make use of one form of Stirling's approximation for large factorials, i.e., $\ln N! \approx N\ln N - N$, we find that

$$f \equiv N e^{-\beta A/N} \tag{10}$$

Equation (10) has been used in calculating Z in this present Note from the given Helmholtz free energy data.

III. Partition Function and Temperature

Some of the calculated logarithms of the partition functions ($\ln f$) as a function of $\ln\beta$, are shown in Fig. 1. The corresponding translational partition functions are shown for comparison. In Fig. 1, we see that $\ln f$ as a function of $\ln\beta$ for 1 and 5 atm, has a continuously turning tangent always concave to the horizontal axis. The curves are for pressures from 1–2000 atm. In all cases, the translational partition function is a straight line with slope $-\frac{5}{2}$; the temperature dependence of the volume has been utilized. It is well-known that the translational partition function f_t is written as

$$f_t(\beta) = \int_0^\infty e^{-\beta\varepsilon} g_1(\varepsilon)\, d\varepsilon = \left(\frac{2\pi m}{h^2\beta}\right)^{3/2} V \tag{11}$$

$f_t(\beta)$ is the Laplace transform of the density of states function $g_1(\varepsilon)$ and (of course) $g_1(\varepsilon)$ is the inverse transform of the partition function, and ε is the kinetic energy. Equation (11) is the basis of a fundamental inverse relationship in statistical thermodynamics. If one knows the Laplace transform [i.e., $f_t(\beta)$], then $g_1(\varepsilon)$ is easily obtained.

In the case of 10 atm, we see essentially the same behavior as for 1 and 5 atm. $\ln f$ for $p = 20$ atm changes from a concave downward function to a concave upward function at $\ln\beta$ approximately equal to 13.7. For $p = 60$, 100, and 120 atm, respectively, the curves show somewhat similar behavior to the curves as low atmospheres; however, they become more like straight lines. The trend is completed for $p = 500$ atm and $p = 2000$ atm.

Somewhat different aspects of this behavior as well as some interpretation of the microscopic behavior will be given in the succeeding paragraphs.

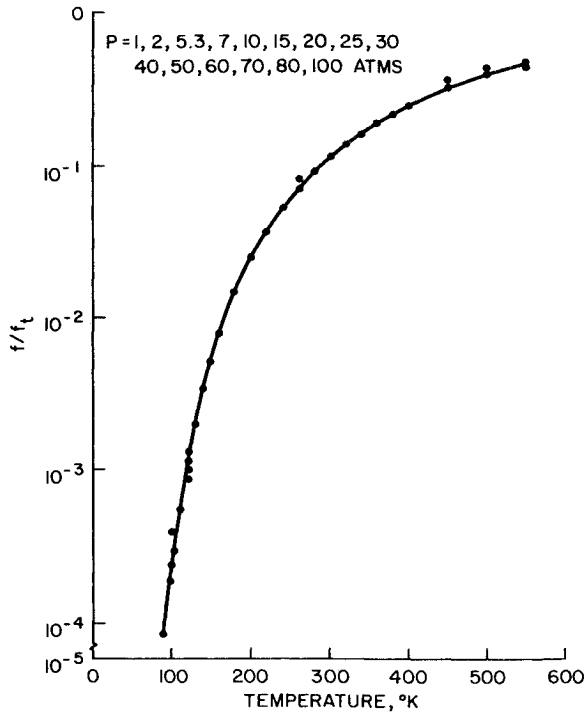

Fig. 2 Ratio of the actual partition function to translation partition function as a function of temperature.

We have used the experimental data to evaluate f, and hence f_c indirectly. We can define $f_c(\beta, p)$ as

$$f_c(\beta, p) = \frac{1}{V}\int \exp[-\beta U_c(\mathbf{r})]\,dr = \frac{f_i(\beta)}{(2\pi m/h^2\beta)^{3/2}V} \tag{12}$$

where the right-hand side is known. In Eq. (12), $U_c(r)$ is the effective potential which one particle sees as the result of its interaction with all of the other particles.[3] Some of the results are shown in Figs. 2 and 3. In Fig. 2, we see that the general trend is for $f_c(\beta, p)$ to increase with decreasing β; in the limit of β approaching zero, $f_c(\beta, p)$ becomes equal to the volume of the container. If the function $U_c(r)$ is negative, then we would expect $f_c(\beta, p)$ to be a decreasing function with decreasing β. Since it is an increasing function as β decreases, this means that in the range of temperatures and pressures studied, the influence of the repulsive part of the potential dominates that of the attractive part.

Robinson[4] has calculated integrals of the type given in $f_c(\beta, p)$ in connection with another problem where the potential function was the Lennard-Jones potential. The general integral was of the form

$$I(x, \varepsilon\beta) = \int_0^\infty t^x e^{-4\varepsilon\beta(t^2 - t)_{dt}} \tag{13}$$

where $V(r) = 4\varepsilon[(\sigma/r)^{12} - (\sigma/r)]^6$ and $(\sigma/r)^6 = t$. It was found out that $I(x, \varepsilon\beta)$ is not a monotone function of $\varepsilon\beta$. In general, it is a decreasing function of $\varepsilon\beta$, but for some ranges of the parameter x and of $\varepsilon\beta$, important in the present problem, $I(x, \varepsilon\beta)$ can increase with increasing $\varepsilon\beta$. In view of the preceding type of behavior, one can account for trends shown in all of the figures.

The behavior of $f_c(\beta, p)$ with pressure, shown in Fig. 3, is not so simple however. In the low temperature range, f_c remains constant and then decreases as the pressure is increased, up to a certain point. Beyond this point, f_c increases with increasing pressure. We see from Fig. 3 that the phenomenon just described occurs in the temperature range from 100°K to about 170°K. At 180°K, the minimum has almost disappeared. At higher temperatures f_c is essentially independent of the pressure. The different behaviors of the integral and the volume with pressure can account for the appearance of the curves in Fig. 3.

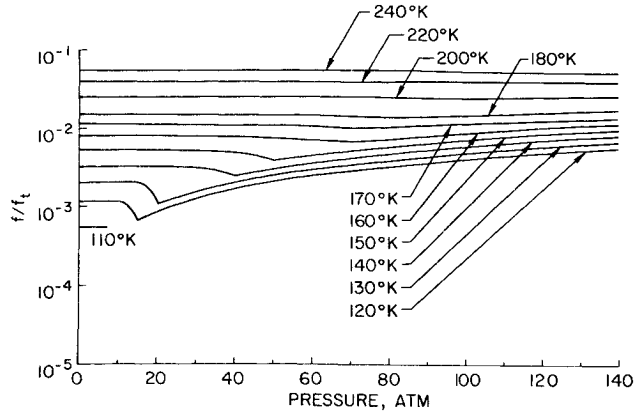

Fig. 3 Ratio of the actual partition function to translation partition function as a function of pressure.

A relatively simple analytical form for the configurational integral f_c can be obtained from curve fitting. The results shown in Fig. 1 can be represented as

$$\frac{1}{V}\int e^{-\beta U_c(r)}\,dr_i = C_1\, e^{-\beta u_o} \exp[-\{C_2(\ln \beta_o/\beta)^2\}] \tag{14}$$

where C_1 and C_2 are positive constant, and u_o and β_o may depend on pressure. If $C_2 = 0$, and $u_o > 0$, then we have the van der Waals case.

We would not expect that the partition function for argon in the temperature and pressure range under discussion to be that of a perfect gas. It is perhaps surprising that the partition function deviates significantly from the trend of a van der Waals gas. The opposite behavior is shown. The partition function for a van der Waals gas is larger than that of the perfect gas in that in Eq. (7) $u_o > 0$ and $C_2 = 0$. The actual partition function, as determined from the experiments is smaller than that of a perfect gas.

IV. Density of States Function for both Kinetic and Potential Energy

We have been able to evaluate the integral in Eq. (6) [strictly speaking, Eq. (12)] from experimental data. The emphasis is now shifted from *evaluating an integral* to the *solution of an integral equation.* Although insufficient data exist for the complete solution of the equation, we shall make some pertinent remarks. The integral

$$Vf_c(\beta, p) = \int_0^\infty e^{-\beta U_c}\,d\mathbf{r}_i \tag{15}$$

can be written as

$$\int_0^\infty e^{-\beta U_c(r)}\,d\mathbf{r} = 4\pi\int_0^\infty \{e^{-\beta x}\}[F(x)]^2\frac{dF(x)}{dx}\,dx \tag{16}$$

In Eq. (16)

$$x = U_c(\mathbf{r}) \tag{17}$$

from which

$$r = [U_c(x)]^{-1} \equiv F(x) \tag{18}$$

and $r^2\,dr = [F(x)]^2(dF/dx)\,dx$. Equation (18) means that r is obtained from inverting (the significance of the -1 exponent) or solving Eq. (17). Finally we can replace the dummy index x in Eq. (16) by u (i.e., potential energy) and get

$$\int_0^\infty e^{-\beta U_c}\,dr = \int_0^\infty e^{-\beta u} g_2(u)\,du \tag{19}$$

where $g_2(u)$, an effective density of states function for potential

energy.‡ From Eq. (16), it is evident that $g_2(u) = 4\pi[F(x)]^2 \times dF(x)/dx$.

In principle, the expression $g_2(u)$ given in Eq. (20) can now be found. We combine Eqs. (14) and (19) and obtain

$$\int_0^\infty e^{-\beta u} g_2(u)\,du = V(\beta, p) C_1 e^{\beta u_0} \exp\left[-\{C_2(\ln \beta_o/\beta)^2\}\right] \quad (20)$$

The inverse transform of the right-hand side of Eq. (20) is $g_2(u)$.

Equations (11) and (19), separately, do not reveal the complete picture. These two equations are connected through Eq. (4); hence the concept of the convolution in Laplace transform theory is pertinent. The product of the two Laplace transforms given in Eqs. (11) and (19) will be called $L_1(\beta)$ and $L_2(\beta)$, respectively. From Laplace transform theory,[5] we have

$$L_1(\beta)L_2(\beta) = \int_0^\infty e^{-\beta E} \int_0^E g_1(E-u)g_2(u)\,du\,dE \quad (21)$$

where $E = \varepsilon + u$. We see that the density of states for a combination of potential and kinetic energy $g(\varepsilon, u)$ is not $g_1(\varepsilon)g_2(u)$ but rather

$$g(\varepsilon, u) = \int_0^E g_1(E-u)g_2(u)\,du = \int_0^E g_1(\varepsilon)g_2(u)\,du = \int_0^E g_2(E-\varepsilon)g_1(\varepsilon)\,d\varepsilon \quad (22)$$

At this time, we shall not attempt to evaluate $g_2(u)$ for argon from the data. We would like to indicate that it can be evaluated from Eqs. (19) and (20). No simple inverse transform of the right-hand side of Eq. (20) is known.

V. Conclusions

In order to utilize inverse relationships, we have determined an analytical form for the partition function for argon gas in the temperature and pressure ranges already specified. Apparently this is the first such listing of an experimental partition function. We find that the partition function for a van der Waals gas inadequate to represent the data. The results tell us that the intermolecular potential for argon gas has a strong repulsive part in the temperature and pressure range under investigation. The equation of state for argon would not reveal the above aspect of the microscopic system. The equation of state could be essentially van der Waals, with the energy aspects of argon being quite different.

The particle partition function is

$$f = (2\pi m/h^2\beta)^{3/2} V_f e^{\alpha\beta} C_1 \exp\left[-C_2(\ln \beta_o/\beta)^2\right] \quad (23)$$

which gives the following expression for the equation of state

$$\frac{pV_f}{kT} = V_f\left\{\frac{1}{V_f} + \beta\frac{\partial\alpha}{\partial V} + \frac{\partial}{\partial V}\left[\left[C_1 \exp\left[-C_2(\ln \beta_o/\beta)^2\right]\right]\right]\right\} \quad (24)$$

The first two terms in the braces constitute the expression for the van der Waals equation of state. If the third term is small, then the equation of state for argon gas is like a van der Waals gas. We did not attempt to investigate the volume (or pressure) dependence of the parameters shown in Eq. (24) and hence can make no remarks in this regard.

References

[1] Din, F., *Thermodynamic Functions of Gases*, Vol. 2, Butterworth, London, 1956.

[2] Eyring, H., Henderson, D., Stover, B. J., and Cyring, E. M., *Statistical Mechanics and Dynamics*, Wiley, New York, 1964, p. 94.

[3] Reif, F., *Fundamentals of Statistical and Thermal Physics*, McGraw-Hill, New York, 1965, p. 426, Eq. (10.5.2).

[4] Robinson, L. B., "Frequency Shifts in the Hyperfine Spectra of Alkalis Caused by Foreign Gases," *Physical Review*, Vol. 117, 1960, p. 1275.

[5] Widler, D. V., *The Laplace Transform*, Princeton Univ. Press, Princeton, N.J., 1946.

‡ Strictly speaking, the right-hand side of Eq. (25) should consist of a linear combination of the types of integral shown. The number of terms is determined by the number of roots of Eqs. (17) or (18). We show only one such term because in the range of temperatures and pressures studied, $\beta U_c(r)$ appears to be a monotone function of r_i.

New Diagnostic Technique for the Study of Turbulent Boundary-Layer Separation

C. C. Horstman* and F. K. Owen†

NASA Ames Research Center, Moffett Field, Calif.

TURBULENT separated flows occur in many types of engineering configurations. They may be unintentional features of some classes of equipment or they may be deliberately introduced. But in all cases such flows can have a significant effect on engineering performance. Furthermore, additional complications are added by the unsteady aspects of the turbulent boundary-layer separation and reattachment processes. Despite the fact that these flows have been extensively studied, detailed information regarding the unsteady nature of turbulent separation is practically nonexistent for high-speed compressible flows. Conventional "time averaged" measurements such as surface pressure, skin-friction, heat-transfer, and pitot pressure surveys cannot supply this information. In this Note, a diagnostic technique is described which provides basic information of the significant unsteady character of turbulent boundary-layer separation. In this technique, thin platinum films are mounted flush with the model surface, and the fluctuating voltages from these films provide measurements related to the flow character above the film. Results are presented for a hypersonic shock-wave turbulent-boundary-layer interaction with and without separation.

The investigation was conducted in the Ames 3.5-ft hypersonic wind tunnel. In this facility, high-pressure heated air flows through the 1.067-m-diam test section to low-pressure spheres. The nominal freestream test conditions were at Mach number 7.2, total pressure of 33 atm, and total temperature equal to 667°K. The test model consisted of a cone-ogive-cylinder, 3-m long and 0.203 m in diameter, with an annular shock wave generator, 0.51 m diam, mounted concentric with the model. The wedge angles of the shock-wave generator were varied from 7.5° to 15° providing a range of shock-wave strengths giving both attached and separated shock-wave boundary-layer interaction flows. The generator was also movable along the cone-ogive-cylinder axis so that the entire interaction region could be passed over a single measurement station on the model. Previous test results[1] without the generator have established the existence of a fully developed, self-similar turbulent boundary layer with negligible pressure gradient from 100 to 300 cm from the model tip. The present measurements were obtained between 180 and 200 cm from the model tip. The measured boundary-layer parameters prior to shock impingement were approximately: edge Mach number of 6.9, boundary-layer thickness of 2.7 cm, Reynolds number based on boundary-layer thickness of 0.2×10^6. The model wall temperature was 310°K. The unsteady aspects of the separated flow region was investigated using thin platinum films deposited on a pyrex glass substrate and mounted flush with the model surface. Gage construction and constant temperature operation were identical to that described in Refs. 2 and 3. The upper frequency limit (−3 db) of the gages, as determined by the conventional square wave technique, was 40 kHz although significant correlations were obtained at frequencies above 65 kHz.

Two typical variations of the rms thin-film voltage fluctuations through the shock-wave boundary-layer interaction region are shown in Fig. 1. Also indicated are the measured pressure

Received March 25, 1974; revision received May 6, 1974.

Index categories: Boundary Layers and Convective Heat Transfer—Turbulent; Supersonic and Hypersonic Flow.

* Assistant Chief, Experimental Fluid Dynamics Branch. Associate Fellow AIAA.

† Consultant; now Senior Research Engineer, United Aircraft Research Laboratories, East Hartford, Conn.